

SST-Forced and Internal Variability of the Atmosphere in an Ensemble GCM Simulation

Shinji MATSUMURA

Faculty of Environmental Earth Science, Hokkaido University, Sapporo, Japan

Gang HUANG

Institute of Atmospheric Physics, Chinese Academy of Sciences, Beijing, China

Shang-Ping XIE

International Pacific Research Center and Department of Meteorology, SOEST, University of Hawaii, Honolulu, USA

and

Koji YAMAZAKI

Faculty of Environmental Earth Science, Hokkaido University, Sapporo, Japan

(Manuscript received 11 July 2005, in final form 29 September 2009)

Abstract

A 20-member ensemble simulation has been conducted with an atmospheric general circulation model to investigate the time-space characteristics of the leading modes of internal and SST-forced variability in the winter Northern Hemisphere. Each of the 20 integrations is forced by the identical global sea surface temperature (SST) and sea ice history observed for 1959–1998, and differs only in the initial conditions. A variance analysis is performed to quantify the relative importance of the SST-forced and internal variability. In the extratropics, the SST-forced signals are much higher in the North Pacific than in the North Atlantic where month-to-month and interannual variability is dominated by internal chaos.

The leading empirical orthogonal function mode resembles the Arctic Oscillation (AO) for both the internal and ensemble-mean variability but with significant differences in correlation between the Pacific and Atlantic centers of action. The Pacific-Atlantic correlation is significantly higher for the ensemble mean than for all but one member integration. The correlation between the Arctic and midlatitude North Atlantic, by contrast, is higher in individual member runs than in the ensemble-mean. These results suggest that SST-forced variability is organized into a hemispheric AO pattern while internal variability is more confined in the North Atlantic sector. Seasonal air-sea interactions in the North Pacific and Atlantic are also discussed.

1. Introduction

The Arctic Oscillation (AO) or the Northern Annular Mode (Thompson and Wallace 1998; Thompson and Wallace 2000) is the leading empir-

ical orthogonal function (EOF) mode of extratropical atmospheric variability with a hemispheric-scale pattern. The AO appears to be an internal mode of the atmosphere as atmospheric general circulation models (AGCMs) produce a mode similar to the observed AO with climatological sea surface temperatures (e.g., Yamazaki and Shinya 1999), but the AO may be modulated by various external forcings of different spatio-temporal structures (Feldstein 2002). The AO pattern is highly corre-

Corresponding author: Shinji Matsumura, Faculty of Environmental Earth Science, Hokkaido University, Kita 10, Nishi 7 Kita-Ku, Sapporo 060-0810, Japan.
E-mail: matsusnj@ees.hokudai.ac.jp
© 2010, Meteorological Society of Japan

lated with the North Atlantic Oscillation (NAO) pattern (e.g., Wallace and Gutzler 1981; Hurrell 1995), raising a question of whether the AO is a physical mode or statistical artifact of the EOF analysis (Deser 2000; Ambaum et al. 2001; Itoh 2002). The pattern differences suggest different underlying physical mechanisms: The sectoral NAO points to a mechanism local to the Atlantic region whereas the AO suggests a hemispheric coherence beyond ocean basins.

Using AGCMs forced by observed, time-varying, sea surface temperature (SST) and sea-ice boundary conditions, several studies showed that the ensemble-mean NAO variability, albeit with reduced amplitudes, correlates reasonably well with observations in the recent three decades, suggesting that the simulated NAO variations are caused by SST variations in the mid-latitude North Atlantic (Rodwell et al. 1999; Mehta et al. 2000) or the tropical oceans (Hoerling et al. 2001). Regarding the atmospheric response to extratropical SST anomalies, the results from AGCM studies are not consistent in all respects but tend to suggest that the response is rather weak relative to internal variability (e.g., Palmer and Sun 1985; Kushnir and Held 1996; Peng et al. 1997). Thus, to reliably study the SST-induced atmospheric variability, we need to consider internal variability. Such information on both types of variability is available from an ensemble of AGCM integrations (e.g., Harzallah and Sadourny 1995; Cassou and Terray 2001; Schneider et al. 2003).

We have conducted a 20-member ensemble of AGCM integrations in order to quantify and characterize the SST-forced variability. The intra-ensemble variance will give the statistics of atmospheric internal variability including its spatial patterns while the ensemble mean will yield SST-forced variability, to the extent that the model is a realistic representation of the atmosphere. The same statistical analysis is applied to observational data to evaluate the degree of realism of the model simulation. The present study is an effort to describe and characterize the model variability over the Northern Hemispheric extratropics in winter, thereby providing a reference for future regional studies.

The rest of the paper is organized as follows. Section 2 describes the model and experiments. Section 3 presents the results from a variance analysis. Section 4 compares the AO mode between the ensemble mean and observations, and discusses the differences in AO's spatial structures between the

internal and SST-forced variability and also discusses the influence of El Niño/the Southern Oscillation (ENSO). Section 5 is a summary.

2. Model and simulation design

The AGCM used in this study was developed jointly by the Center for Climate System Research (CCSR) of the University of Tokyo and the National Institute for Environmental Studies (NIES) in Japan. This model is a global spectral model with the sigma coordinate in the vertical. Details of model physics and its performance may be found in Numaguti et al. (1997) and Numaguti (1999). Here we employ a version with triangle truncation at zonal wavenumber 21 (T21), and 20 sigma levels. By today's standard, this resolution is rather low, a compromise for a relatively large ensemble. The low resolution probably may lead to an underestimate of atmospheric variability, both internal and SST-forced, but our limited comparison with regard to North-Atlantic variability indicates that the spatial patterns are rather similar between T21 and T42 runs (Okumura and Xie 2003).

Yamazaki and Shinya (1999) reported the success in simulating the AO pattern in space in a 40-year run of this AGCM forced by the climatological SST and sea ice. Here we have carried out ensemble integrations as follows. First the model was spun up for 20 years under the climatological SST and sea ice boundary conditions. Then SST and sea ice fraction are replaced with the observed history based on the GISST2.3b dataset (Rayner et al. 1996) for 1959–1998, and the model is integrated for this 40-year period. A total of 20 runs was performed and each run is initialized by one of the January 1 fields from the 20-year spin-up run. These 20 hindcast runs for 1959–1998 are otherwise identical. We take the ensemble mean as SST-forced signal while the intra-ensemble differences as due to internal variability of the atmosphere. As will be seen, the initial condition differences lead to large differences among the ensemble members. For validation, we use the National Centers for Environmental Prediction (NCEP) and National Center for Atmospheric Research (NCAR) reanalysis (Kalnay et al. 1996), available on a 2.5° grid in the horizontal.

3. SST-forced and internal variability

3.1 Variance analysis

To quantify the relative magnitude of the SST-forced and internal variability, we use the variance

analysis proposed by Rowell et al. (1995). This statistical method partitions the total variance of a given field into two components: the externally forced variability and chaotic variability generated internally by the model. Since each ensemble member is subject to the same SST forcing, the spread among the members ($\hat{\sigma}_{INT}^2$) represents the internal variability and variance of the ensemble average ($\hat{\sigma}_{EM}^2$) represents the SST-forced variability. However, the latter may include a non-negligible influence of internal variability and therefore overestimate the SST-forced variability unless a proper correction is made. The unbiased estimate including such a correction of the SST-forced variability ($\hat{\sigma}_{SST}^2$) is calculated as follows (Rowell et al. 1995).

$$\hat{\sigma}_{INT}^2 = \frac{1}{N(n-1)} \sum_{i=1}^N \sum_{j=1}^n (x_{ij} - \bar{x}_i)^2, \quad (1)$$

$$\hat{\sigma}_{EM}^2 = \frac{1}{(N-1)} \sum_{i=1}^N (\bar{x}_i - \bar{\bar{x}})^2, \quad (2)$$

$$\hat{\sigma}_{SST}^2 = \hat{\sigma}_{EM}^2 - \frac{1}{n} \hat{\sigma}_{INT}^2. \quad (3)$$

Here, $\hat{\cdot}$ denotes the best estimator of a population quantity, where N and n are the number of years and the ensemble size, respectively, x_{ij} represents the data of the i -th year and j -th member of the ensemble, \bar{x}_i is the ensemble mean of the i -th year, and $\bar{\bar{x}}$ is the mean of all data. The variance ratio is used as a measure of the potential predictability as

$$\hat{R} = \frac{\hat{\sigma}_{SST}^2}{\hat{\sigma}_{TOT}^2}, \quad (4)$$

where $\hat{\sigma}_{TOT}^2 = \hat{\sigma}_{SST}^2 + \hat{\sigma}_{INT}^2$ is the unbiased estimate for the total variability. The interaction between internal and external variability is generally weak in our variance analysis while in reality, SST-induced changes in atmospheric circulation may have a significant impact on internal variability (e.g., Quadrelli and Wallace 2002).

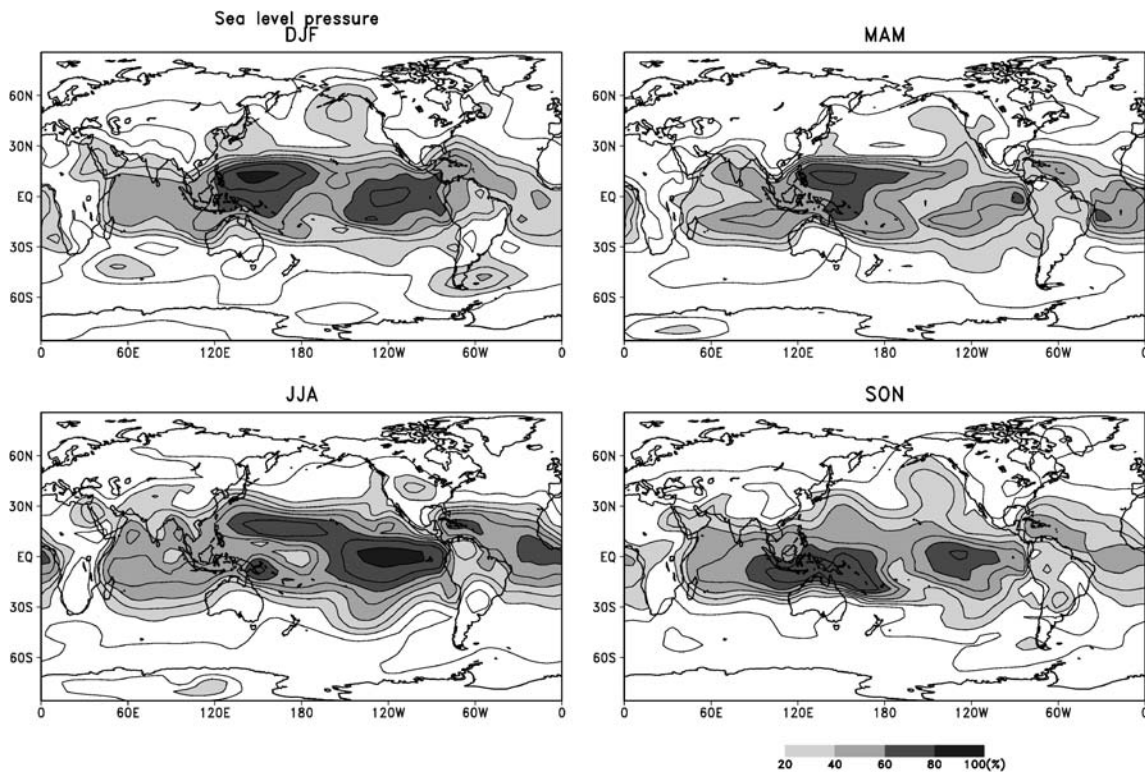


Fig. 1. Percentage of the variance of seasonal SLP due to oceanic forcing. Results for each of four standard seasons are shown. The contour interval is 10% and the areas over 10% are significantly different from zero at the 95% confidence level with an F test.

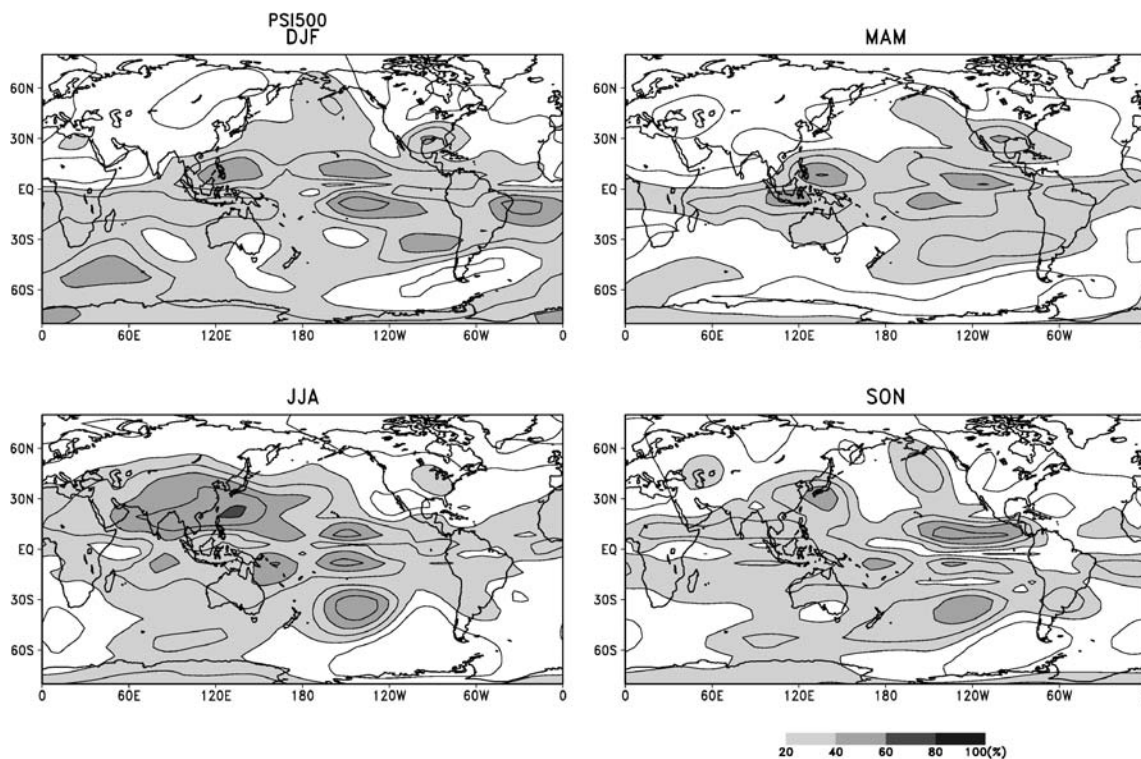


Fig. 2. Same as in Fig. 1, but for 500 hPa stream function field.

3.2 Potential predictability

a. Seasonal potential predictability

The forced-to-internal variance ratio represents the potential predictability due to slow SST forcing. Figure 1 displays the estimated potential predictability for sea level pressure (SLP) for four seasons of DJF, MAM, JJA, and SON. In general, the variance ratio is high over the Tropics where the SST forcing is dominant while the ratio is low and there is much chaotic variability in the extratropics (cf. Sugi et al. 1997; Rowell 1998; Cassou and Terray 2001). In the Northern Hemisphere extratropics during DJF, the variance ratio is higher over the oceans than over land. Relatively large values of about 20% are found over the North Pacific extending over Alaska because of the ENSO-induced teleconnection (Section 4.4). The predictability is lower over the North Atlantic except over the Gulf Stream extension region where the local maximum in predictability is comparable to that over the Kuroshio Extension. The high variance ratio over the Aleutian low region due to the ENSO teleconnection is visible in fall and winter seasons but weakens as the season progresses into spring and summer. During JJA and poleward of 30°N, the

variance ratio is high over central North America and north of India but low over the oceans.

Similarly, Fig. 2 shows the variance ratio for 500 hPa stream function, which captures non-divergent/geostrophic flow. Potential predictability over the Tropics is weak compared with Fig. 1 because the flow there is divergent and baroclinic. The predictability is lower over the Northern Hemisphere western boundary current extensions compared with SLP. Therefore, the local maxima in SLP predictability may be a baroclinic response to SST variability induced by changes in major ocean currents (B. Taguchi and N. Schneider, pers. comm.). Such current-induced SST anomalies are strong in late winter when the mixed layer is deep but weak in other seasons (Xie et al. 2000; Schneider and Miller 2001). As in Fig. 1, predictability is high over the Aleutian low region during all seasons other than summer. High predictability over the summer (JJA) subtropical Asia appears even more pronounced than in SLP.

Over the Northern Hemispheric extratropical continents, summer climate is slightly more predictable presumably because of tropical SST influences on monsoon. Over the oceans, conversely, the win-

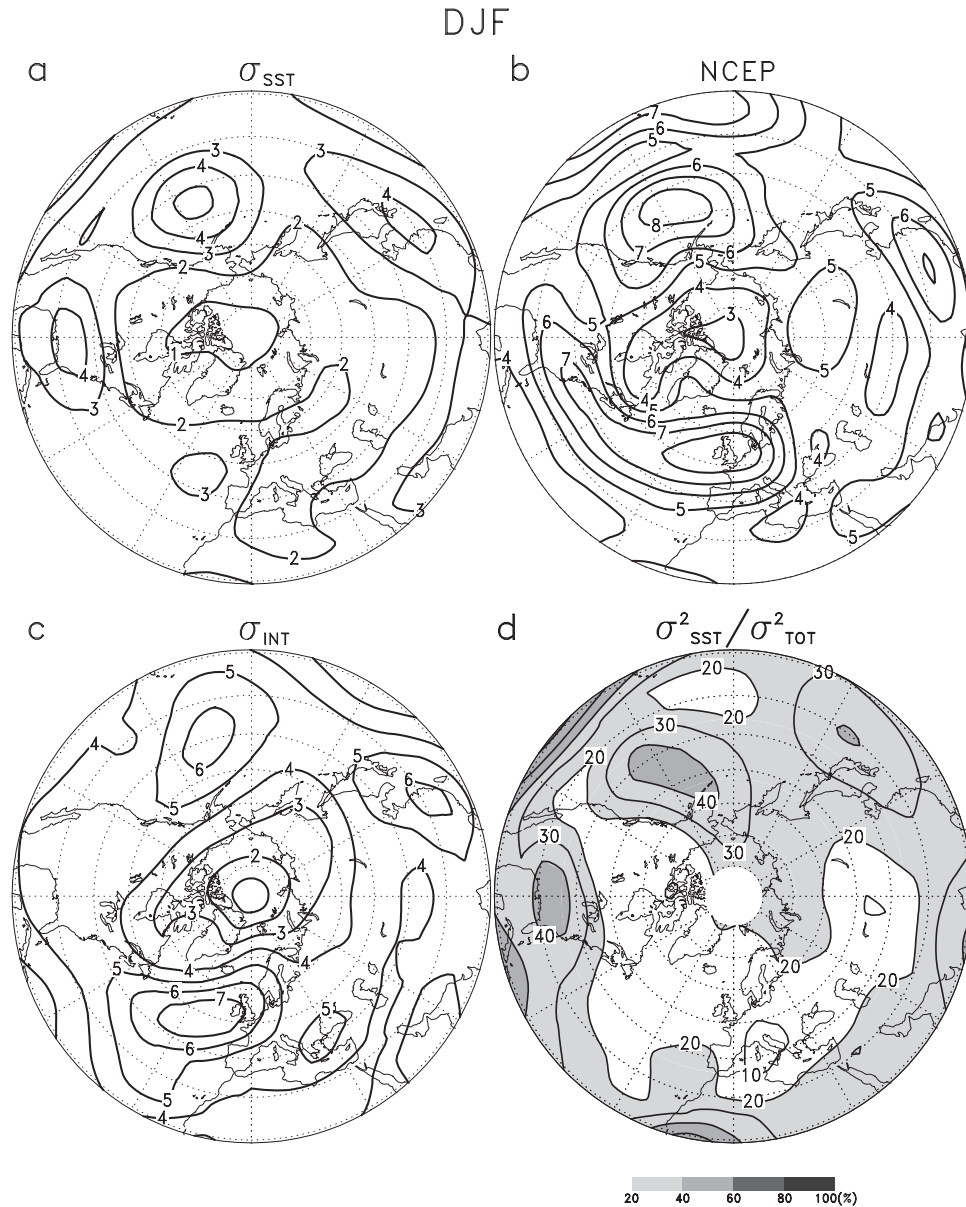


Fig. 3. Standard deviation of 250 hPa stream function ($\times 10^6 \text{ m}^2 \text{ s}^{-1}$) in winter (DJF): (a) $\hat{\sigma}_{SST}$, (b) NCEP, (c) $\hat{\sigma}_{INT}$, and (d) Percentage of the variance.

ter climate is more predictable, often as a result of atmospheric teleconnection from the tropics. In the rest of the paper, we focus on the winter, the season when both the AO and tropical-to-extratropical teleconnection are most pronounced.

b. Winter variability

Figure 3 shows the standard deviation of 250 hPa stream function in the Northern Hemi-

sphere during DJF. As will be seen in Section 4.4, large SST-forced variance over the northeastern Pacific and southeast US is due to the Pacific North American pattern as part of ENSO teleconnection. With the exception of the southeast US maximum, all other maxima in SST-induced variance are roughly collocated with those in internal variance. Using the same AGCM, Okumura et al. (2001) show that tropical Atlantic SST anomalies induce

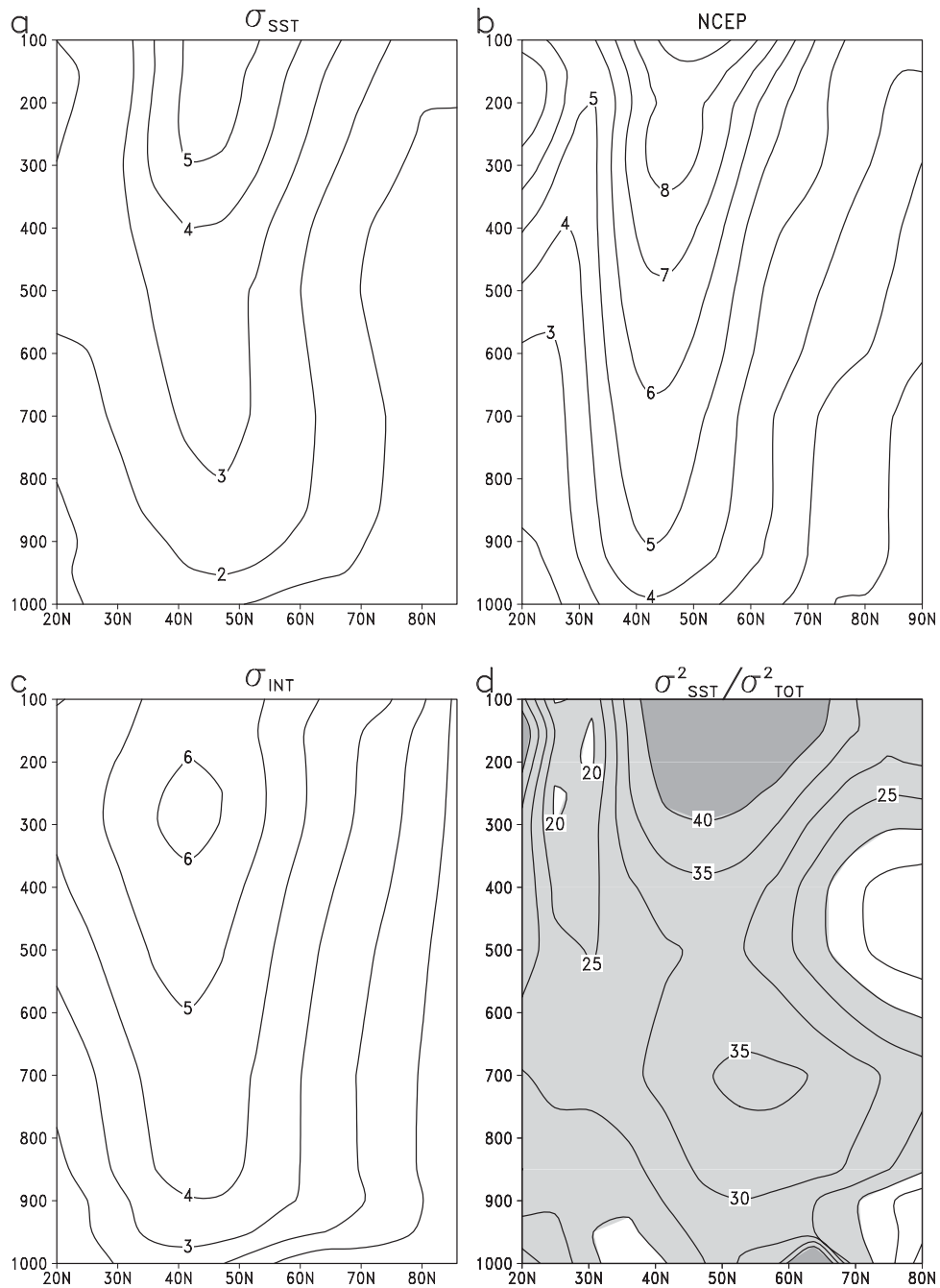


Fig. 4. Same as in Fig. 3 but for vertical sections at 160°W over the Pacific.

NAO-like response in the North Atlantic, with large height anomalies in a mid-latitude region roughly coincident with the maximum in SST-induced variance west of South Europe. The maximum in SST-induced variance over East Asia is due to tropical Pacific SST anomalies (e.g., Kitoh 1988).

Overall the total variance ($\hat{\sigma}_{TOT}$) compares quite well with the NCEP reanalysis variance, both in spatial pattern and in magnitude (not shown). To the extent that the model is realistic, roughly half of the observed variance is due to SST forcing in the PNA's two centers of action over the northeastern Pacific and southeast US. Over the extratropi-

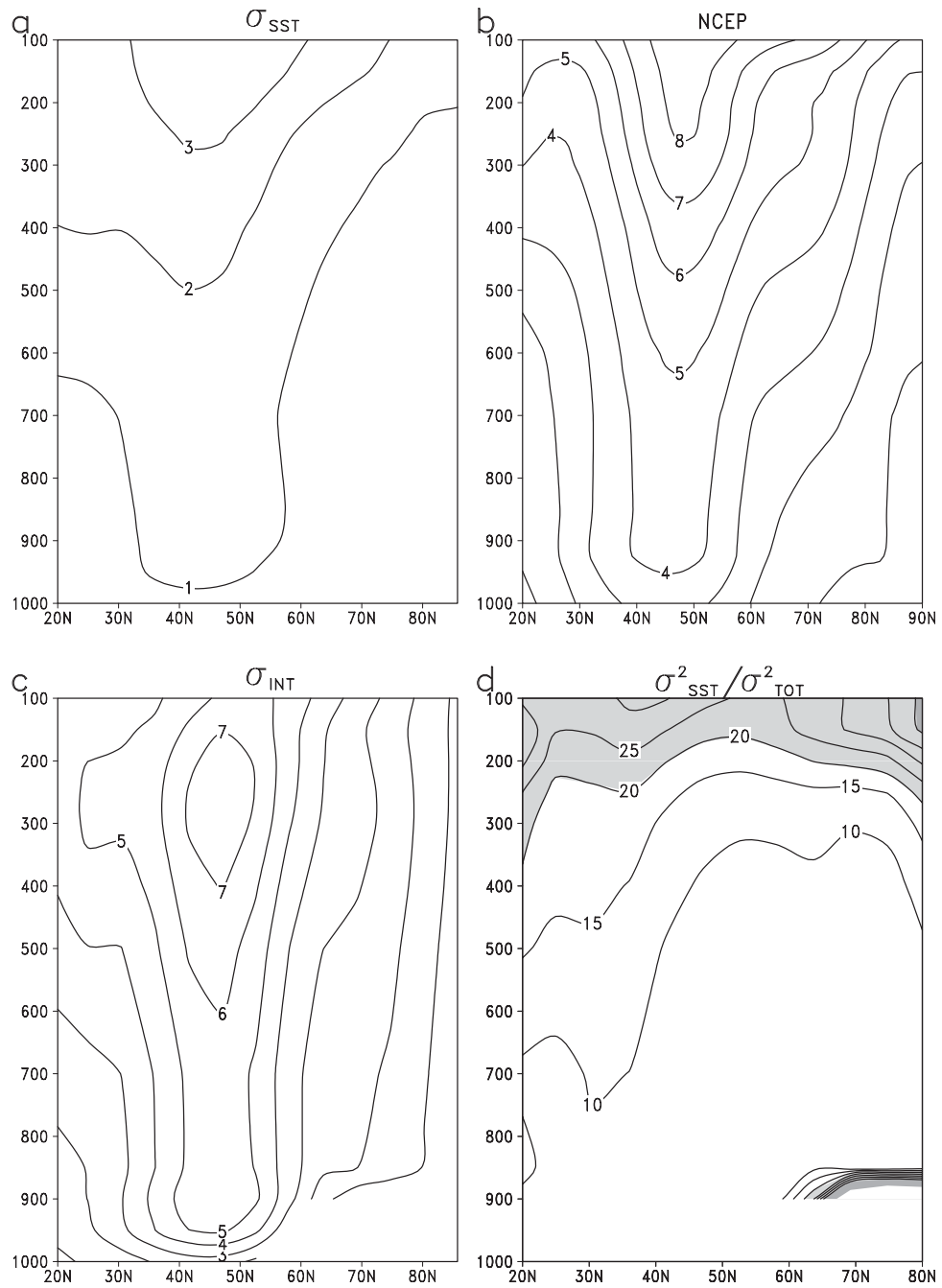


Fig. 5. Same as in Fig. 4 but for at 30°W over the Atlantic.

cal Atlantic, the overwhelming majority of the observed variance appears due to internal variability. Along the NCEP variance maximum over the mid-latitude North Atlantic, in particular, the western portion over the southeast US and western Atlantic is due to the ENSO-induced PNA while the eastern

portion is due to chaotic variability with a small contribution from tropical Atlantic SST.

To further examine the variance maxima over the North Pacific and North Atlantic, Figs. 4, 5 show meridional transects across these centers of action. Along 160°W, variance peaks at 250 hPa,

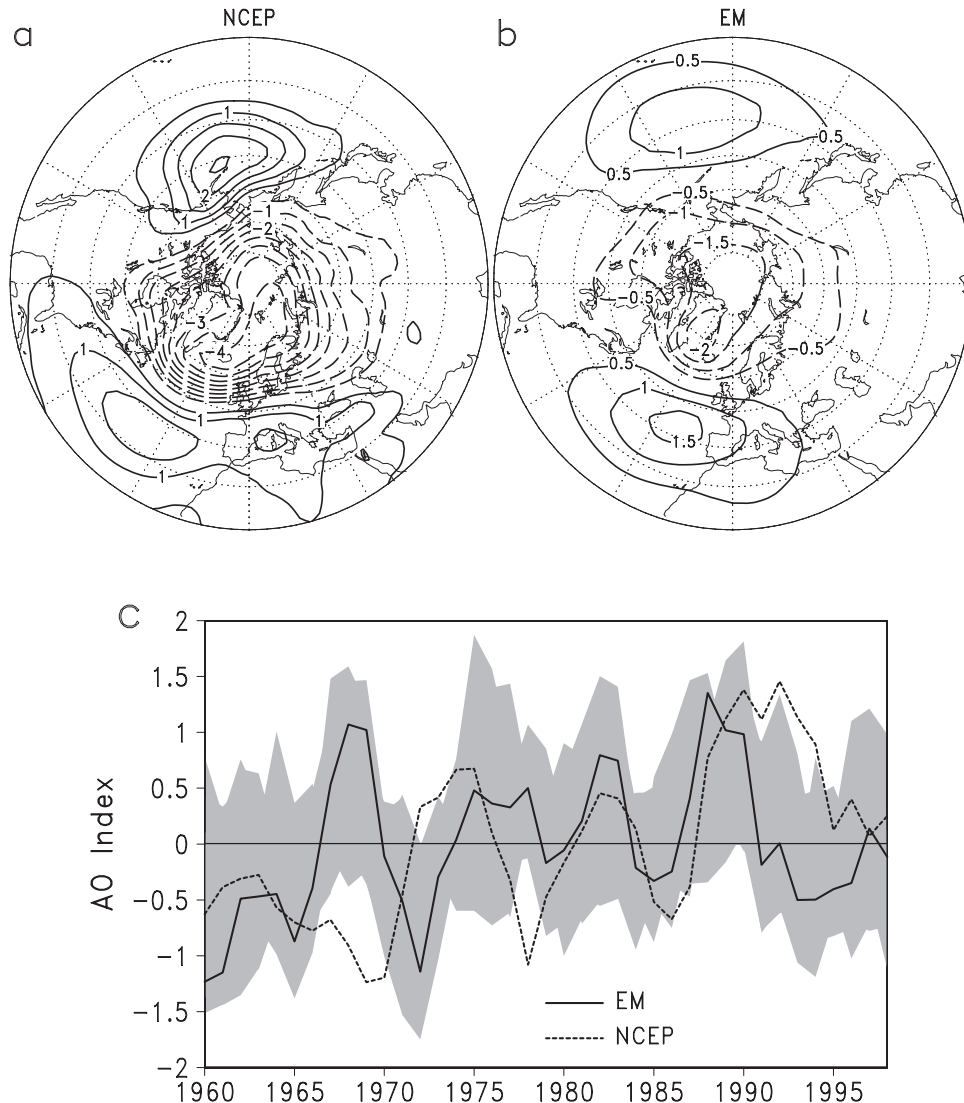


Fig. 6. EOF-1 of SLP anomalies (hPa) for DJF-mean poleward of 20°N for (a) NCEP and (b) ensemble mean (EM). The contour interval is 0.5 hPa with the zero contour omitted. (c): The associated principal components for EM (thick line), each 20-member experiment (shading) and NCEP (dashed line). All time series are normalized and denote a three-year running filter emphasizing the decadal time scale.

40°N , where the westerly jet lies. The SST-forced variability (Fig. 4a) is similar in distribution of the observed variability (Fig. 4b), and so is the internal variability (Fig. 4c). SST-induced variability and internal variability are comparable in magnitude. Therefore, both the SST-forced variability and internal variability contribute to the variability in the North Pacific. Along 30°W in the North Atlantic, internal variability is much greater than SST-forced variability, and comparable to the NCEP variance. Thus, the North Pacific winter climate is highly pre-

dictable (Fig. 4d) over the entire troposphere while the extratropical North Atlantic is dominated by internal variability of the atmosphere.

4. Behavior of the AO in the SST-forced and internal variability of the atmosphere

4.1 The simulated AO

In this section, we investigate the leading modes of atmospheric variability as represented by the EOF analysis. Figure 6 shows the first EOF of NCEP reanalysis and ensemble-mean (EM)

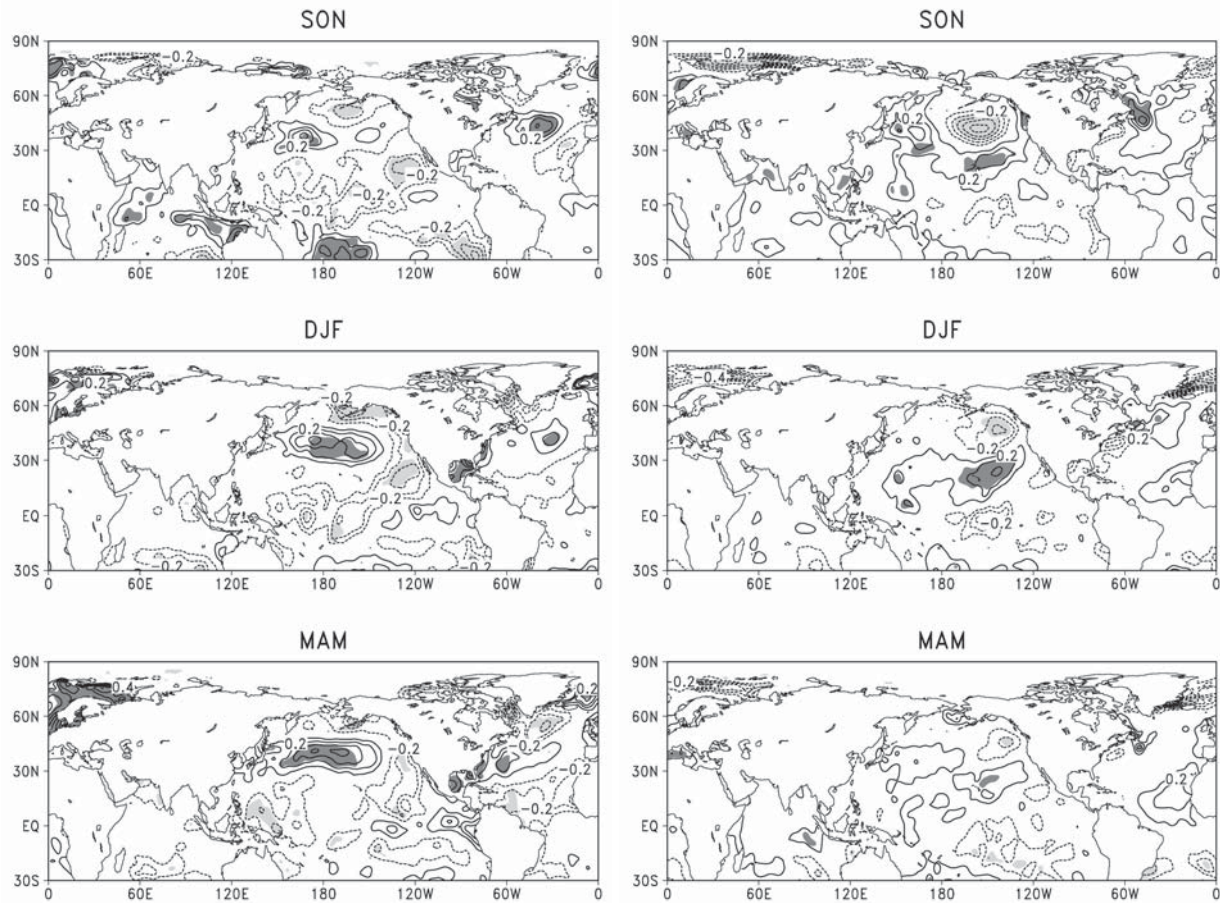


Fig. 7. Seasonal SSTs regression onto the band-passed decadal winter SLP EOF-1 for NCEP (left panels) and EM (right panels) in autumn (SON), winter (DJF), and spring (MAM). The contour interval is 0.1°C with the zero contour omitted, and areas above the 95% significance limit based on a t test are shaded.

anomalies of SLP for DJF-mean and the principal component time series. Throughout this chapter, EOF analyses are performed over the Northern Hemisphere north of 20°N . Each EOF-1 accounts for 50.8% (NCEP) and 46% (EM) of the total variance and represents the AO-like patterns, with three centers of action over the Arctic, mid-latitude North Atlantic and Pacific. The three-month mean NCEP-AO shows a stronger signal in the Pacific than Thompson and Wallace's (1998) monthly AO. The NCEP-AO also seems to resemble the seesaw relationship between the Aleutian and Icelandic lows (Honda and Nakamura 2001).

Figure 6c compares the normalized principal components (PCs) between EM with a range of the 20 individual runs (shading) and NCEP reanalysis. (The absolute variance is much larger in observations than in EM.) The NCEP-PC shows an up-

ward trend, which is missing in the EM simulation. The EM-PC seems to capture the quasi-decadal oscillation for the recent three decades, but the correlation coefficients between two time series are small for their lag oscillation. Xie et al. (1999) note this quasi-decadal oscillation in NAO and show that its pattern is hemispheric bearing a strong resemblance to the TW's AO, in contrast to the interannual NAO that is sectoral. Our EM simulation suggests that the quasi-decadal oscillation during 1970s–1990s is partly forced by SST variations.

4.2 Influence of the SST-forced variability

Figure 7 shows seasonal SST anomalies regressed upon the winter AO principal component with a 3–10 yr band-passed filter. If we assume the three-year averaging reduces the data sample size (39) by a factor of three, the 95% significance level is 0.55

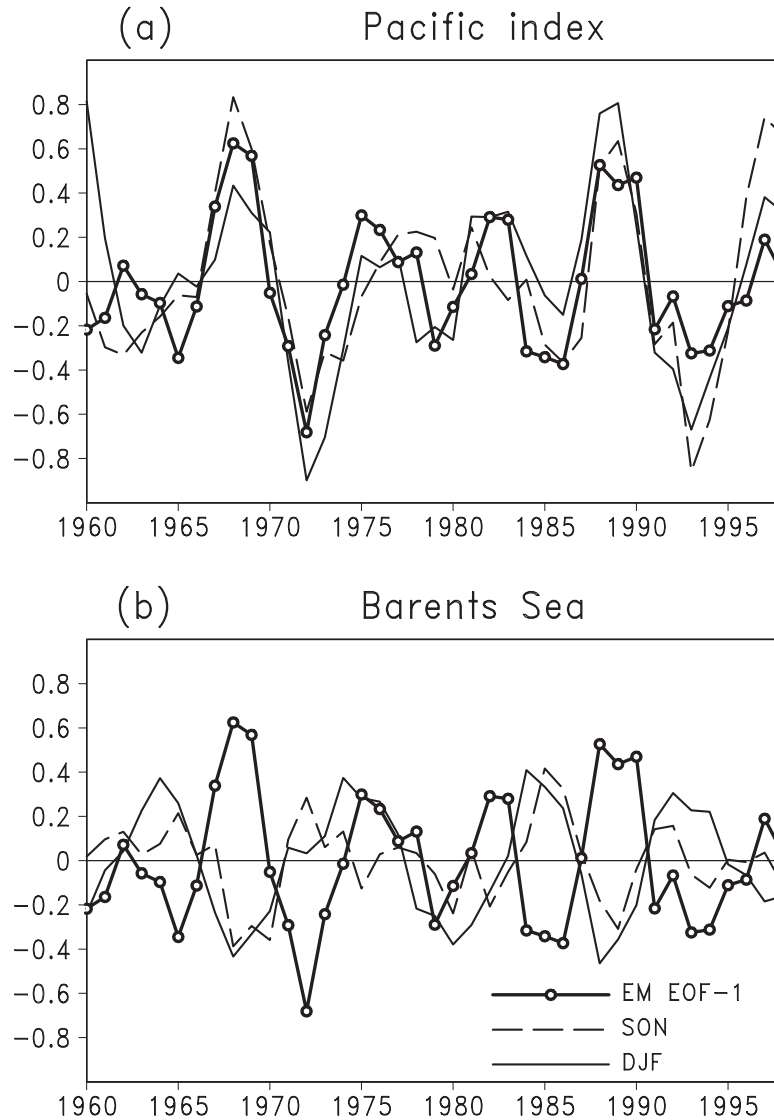


Fig. 8. Band-passed SSTs ($^{\circ}\text{C}$) anomalies in SON (dashed line) and DJF (solid line) averaged over (a) Pacific index (See the text for details) and (b) Barents Sea (30°E – 60°E , 70°N – 80°N) along with the winter EM-AO (thick line with open circle). The winter EM-AO is scaled to facilitate comparison.

based on the t test with reduced freedom (11). The SST regression patterns in observations include two components, both the SST-forced AO and the AO-forced SST variability, but the EM simulation is only forced by SST variations. In SON (Fig. 7, top), the SST signals may be explained by the SST-to-atmosphere forcing both in the NCEP- and in the EM-AO because the SST leads the atmosphere. In DJF (Fig. 7, middle), they show the two-way interaction between the SST and atmosphere in the NCEP-AO, and the SST-to-atmosphere forcing in the EM-AO. In MAM (Fig. 7, bottom), they main-

ly show the atmosphere-to-SST forcing in the NCEP-AO, while signals in the EM-AO merely show the SST-persistence of the previous season.

We focus on the North Pacific and Barents Sea, where the strong SST signals are found in both observations and EM. In the North Pacific the SST regression pattern especially resembles that of the Pacific Decadal Oscillation from winter to spring in observations but is displaced southward from autumn to winter in the EM simulation. For our low resolution model, their difference of the SST signals may reflect the Pacific EM-AO shifts southward

Table 1. Correlation coefficients of seasonal SST (Barents Sea and Pacific index) with the band-passed decadal winter AO index (NCEP and EM). The correlation values above the 95% significance level are in bold type.

	Barents Sea		Pacific index
	NCEP	EM	EM
Autumn (SON)	-0.01	-0.63	0.72
Winter (DJF)	0.25	-0.53	0.65
Spring (MAM)	0.56	-0.35	0.37

than the NCEP-AO (Fig. 6). While the winter NCEP-AO can be forced by autumn SST variability, the winter EM-AO cannot be forced by spring SST variability.

To better confirm the SST-forced response associated with the winter AO, we show in Fig. 8a the time series of seasonal SST anomalies averaged over Pacific sector along with the winter AO. The Pacific index indicates the SST difference of southern part (160°W – 130°W , 20°N – 30°N) and northern part (160°W – 130°W , 40°N – 50°N) in Fig. 7 (EM). The EM-AO is well correlated with the Pacific index, and its correlation coefficients are decreased as the season progresses (Table 1). These results suggest that the winter AO seems to be forced by the North Pacific SST variability in autumn and winter, but also forces the North Pacific SST in winter and spring.

The SST regression patterns for the EM-AO show the negative values in the Barents Sea throughout three seasons (Fig. 7, right), though the correlation coefficients are decreased as the season progresses (Table 1). This is clearly seen by the time-series of the Barents Sea (30°E – 60°E , 70°N – 80°N) SST and that of the EM-AO shown in Fig. 8b. On the other hand, the SST regression patterns for the NCEP-AO in the Barents Sea SST show the negative values in SON, but turn to be positive in MAM (Fig. 7, left). From these results, it is suggested that the cold SST in the Barents Sea in autumn and winter seems to force the positive AO in winter, and the positive AO forces the warm SST in the Barents Sea in spring.

Next, we examine the sea-ice cover regression on the AO (Fig. 9). For the EM, positive regression values are seen in the Barents-Kara and Greenland Seas throughout three seasons, though the values in the Barents-Kara Seas are decreased as the season progresses (Fig. 9, right). It suggests that the heavy sea-ice cover in Barents-Kara Seas in autumn

forces the positive AO in winter, which is similar to the results of Honda et al. (2009). In the observations (NCEP, Fig. 9, left), the weak positive regression patterns in the Barents-Kara Seas are barely seen in SON, but they change the signs in DJF and MAM. In the Greenland Sea, the negative values appear in DJF and MAM, and in the Labrador Sea the significant positive values appear in DJF and MAM. This sea-ice variability is forced by the atmospheric circulation of the AO/NAO (e.g., Deser et al. 2000). The positive AO/NAO generates the negative sea-ice cover in the Barents-Kara and Greenland Seas, which forces the negative AO/NAO. Namely, there is a negative feedback between the AO/NAO and the sea-ice cover in the Barents-Kara and Greenland Seas, which is consistent with the SST-AO relations shown in Figs. 7, 8b, and also consistent with Alexander et al. (2004) and Yamamoto et al. (2006). In summary, the winter AO is forced by the Barents-Kara sea-ice and Barents SST anomalies in autumn, but also the winter AO forces the sea-ice cover and SST in winter and spring.

Let's consider the internal variability of NAO in our simulation where the SST and sea-ice cover are prescribed. In the real world, the negative feedback exists between the SST/sea-ice and the NAO, while no negative feedback exists in the simulation. Therefore, it is expected that the simulated NAO would last longer, and, as a result, the simulated internal NAO variability becomes large due to lack of the negative feedback. This point will be discussed later.

4.3 Influence of the atmospheric internal variability

Table 2 shows the standard deviations and variance ratio of SLP among AO's three centers of action, the Arctic (30°W , 70°N), Atlantic (30°W , 40°N) and Pacific (170°W , 40°N). The internal variability at all these locations is much larger than the SST-forced variability. Their difference is the smallest in the Pacific center, with a variance ratio above 20%. Figure 10 shows the time series of EM SLP at AO's three centers of action, along the first principal component (PC-1). The PC-1's correlation coefficients are -0.9 with the Arctic, 0.65 with the Atlantic, and 0.48 with the Pacific center.

Deser (2000) performed a correlation analysis on SLP among AO's three centers of action using the NCEP reanalysis. The correlation coefficient between the Arctic and Atlantic centers is quite high,

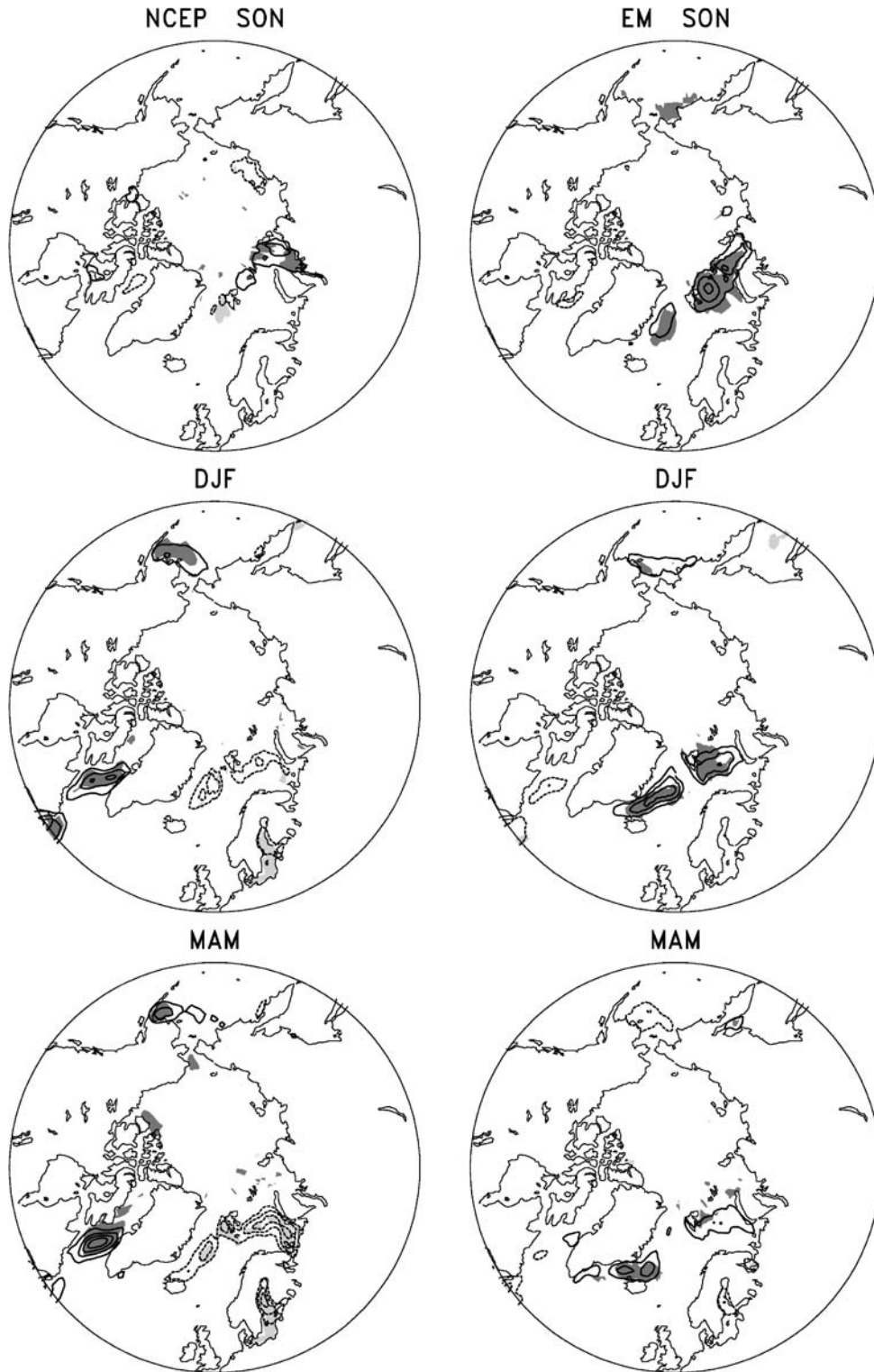


Fig. 9. Same as in Fig. 7, but for sea-ice cover. The contour interval is 5% with the zero contour omitted.

Table 2. Standard deviation (hPa) at AO's three centers of action of SLP for NCEP, σ_{SST} and σ_{INT} . Column 4 represents the percentage of the SST-forced variance, with the bold type denoting numbers significantly different from zero at the 95% confidence level based on an F test.

	NCEP	σ_{SST}	σ_{INT}	$\sigma_{SST}^2/\sigma_{TOT}^2$
Arctic	5.2	1.7	7.8	4.3
Atlantic	4.2	1.5	5.5	7.0
Pacific	5.2	2.3	4.2	23.6

but rather low and insignificant between the Pacific and Atlantic centers. We perform the same analysis for each of the 20 individual member integrations (Fig. 11). Black circles are for correlations between the Arctic and Atlantic sectors, grey circles between the Arctic and Pacific sectors, and opened circles between the Atlantic and Pacific sectors. Correlations between the North Atlantic and Arctic are the highest, like a typical signature of the NAO,

while those between the Atlantic and Pacific are the lowest, similar to the results of Deser (2000). The Pacific correlations for the EM, however, are significantly higher with both the Atlantic and the Arctic. (The Atlantic-Arctic correlations in individual member integrations are similar to that for EM.) The Arctic-Pacific high correlations may mean the existence of seesaw relationship between the Aleutian and Icelandic lows. In all but one member integration, the Pacific-Atlantic correlation is weaker than that for the EM.

Figure 12 compares the EOF-1 and standard deviation between Run-8 (the only run with greater Pacific-Atlantic correlation than in EM) and Run-9 (with reduced Pacific-Atlantic correlation). While remaining about the same over the North Atlantic, the variance of 250 hPa stream function over the North Pacific is noticeably greater in Run-8 than Run-9. Correspondingly, the North Pacific loading of the SLP EOF-1 is greater by more than a factor of 2 in Run-8 than Run-9.

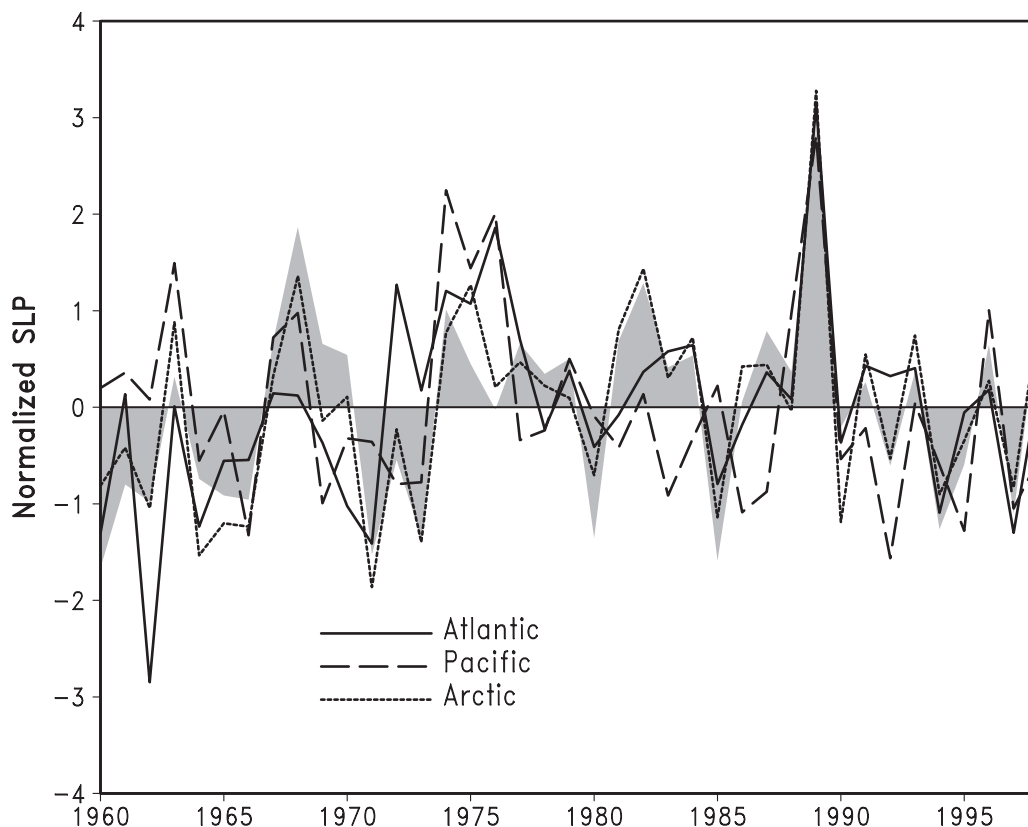


Fig. 10. Time series of SLP at AO's three centers of action, along with the EM EOF-1 (shading). All data are normalized and the Arctic curve is inverted.

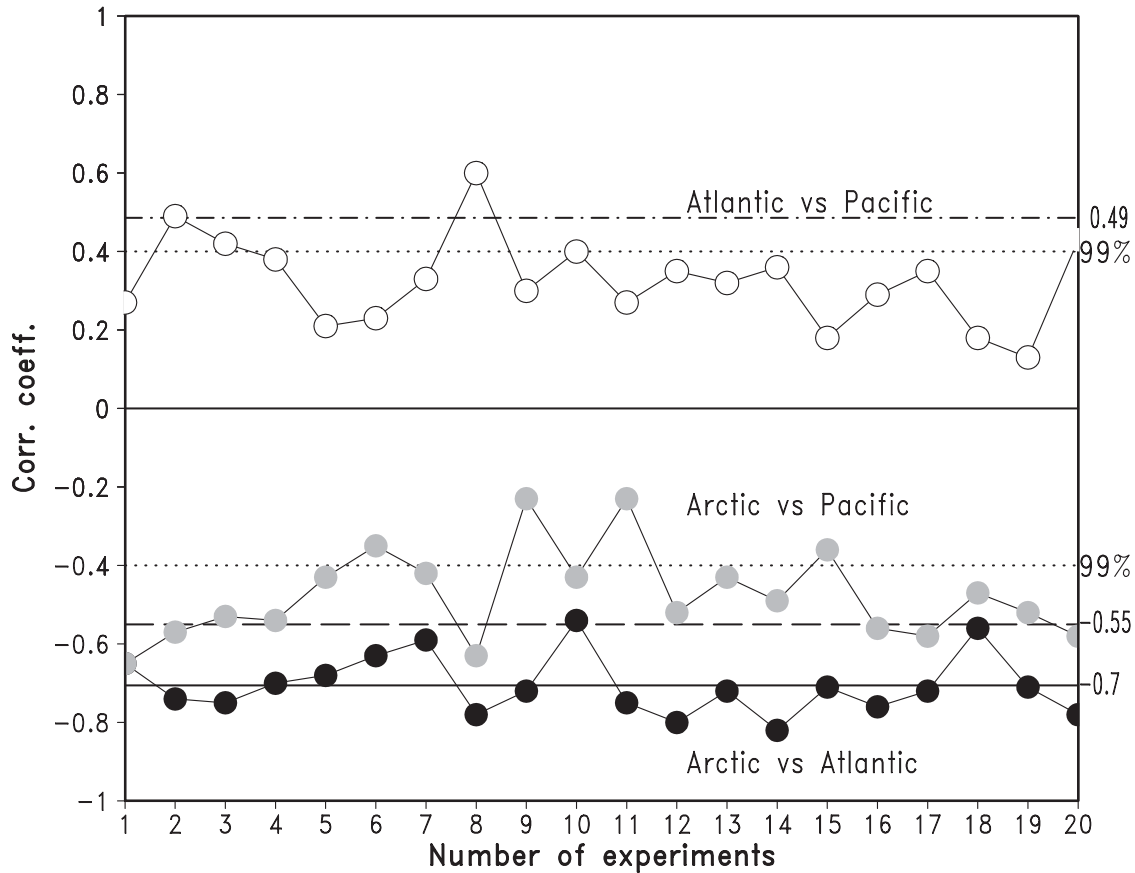


Fig. 11. Correlation coefficients among AO's three centers of action in the 20 members. Black circles are between the Arctic and Atlantic, gray circles between the Arctic and Pacific, and open circles between the Atlantic and Pacific centers. Solid, dashed and dash-dotted lines denote correspondence to correlations in the ensemble mean. A correlation coefficient exceeding 0.4 is significantly different from zero at the 99% confidence level.

Figure 13a shows the EOF-1 for SLP based on the data of all 20-member runs with the EM being subtracted each run (INT), representing the dominant atmospheric internal variability, which accounts for 42% of the total variance. While the loading ratio between the Atlantic and Arctic is similar between the EM (Fig. 13b) and INT, the Pacific-to-Atlantic loading ratio decreases by one third in the latter compared to the EOF for EM. This decreased loading at the Pacific center is consistent with the decreased Pacific-Atlantic correlation in individual member integrations compared to EM. Table 3 shows the maximum (minimum) in SLP EOF-1 (hPa) for the EM, INT, and the ratio between the EM and total variance. The INT at all these locations is much larger than the EM as well

as the SLP standard deviation (Table 2). Their difference is also the smallest in the Pacific center, with a variance ratio above 30%. Thus, SST forcing increases the variance at the Pacific center of action relative to the Atlantic as well as their correlation. As discussed in previous subsection, however, the negative feedback between the NAO and sea-ice variability acts over the North Atlantic sector in winter (e.g., Alexander et al. 2004). Consequently, while the EM-AO weakens in the NAO sector (Fig. 13b), the INT-AO is strengthened (Fig. 13a) because the negative feedback cannot act over the NAO sector.

The vertical structures of the zonal-mean zonal wind anomalies regressed on the INT-AO and EM-AO (Figs. 13c, d) are similar to Thompson

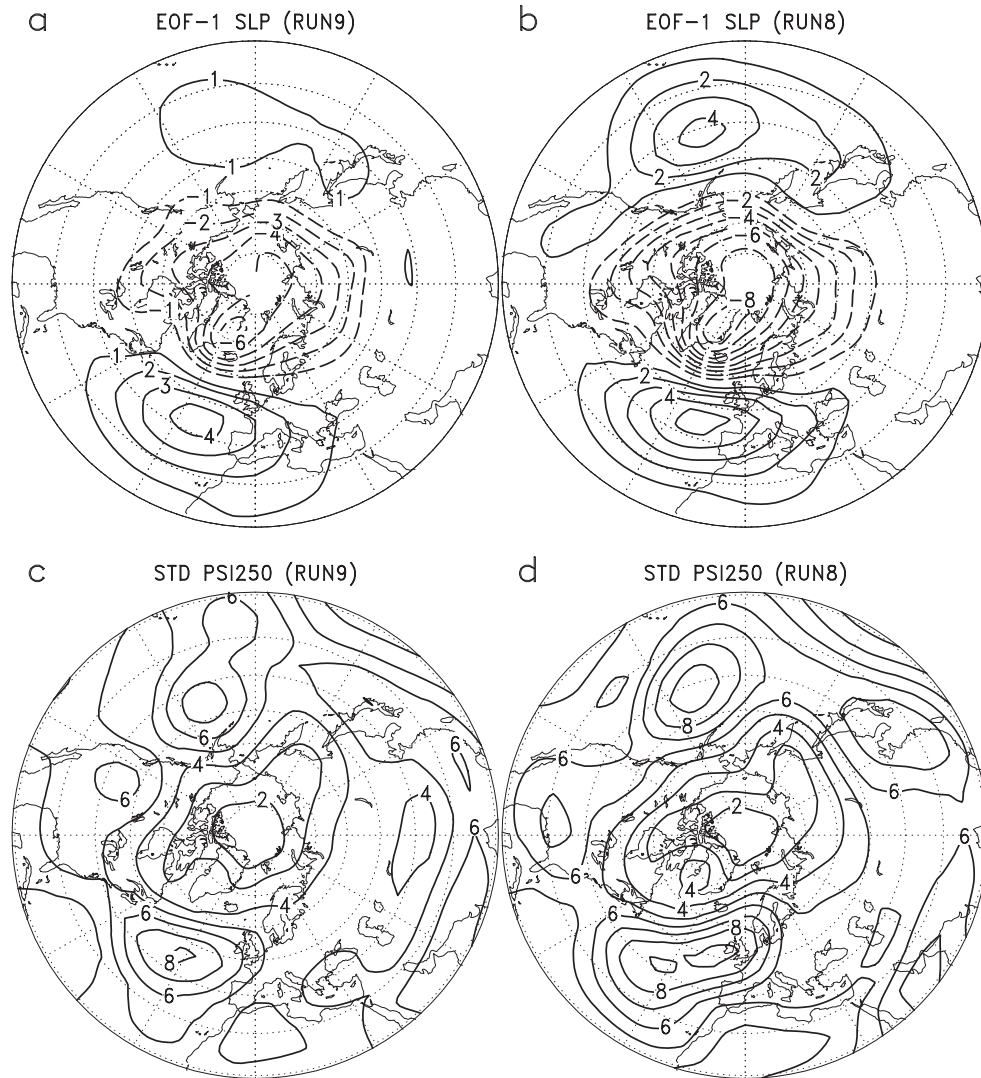


Fig. 12. EOF-1 of SLP anomalies (hPa) for DJF-mean poleward of 20°N in the (a) Run-9 and (b) Run-8. Standard deviation of 250 hPa stream function ($\times 10^6 \text{ m}^2 \text{ s}^{-1}$) in the (c) Run-9 and (d) Run-8.

and Wallace's AO (Thompson and Wallace 2000). The INT high-latitude anomalies are much larger than the EM, whereas those of mid-latitude are comparable in magnitude. The EM mid-latitude centers of action have maxima centered near 20°N in the upper troposphere while the INT mid-latitude centers of action are not clear.

4.4 ENSO influence

Figure 14a shows the 500 hPa geopotential height regressed on the SLP EOF-2 for the ensemble mean. The 500 hPa level is chosen to best show the propagation of barotropic planetary waves. This EOF explains 22% of the total variance, fea-

turing the PNA-like wave-train pattern with centers of action over the Northeastern Pacific, western Canada and southeast US, while there is no signal of the PNA-like pattern in the INT EOF-2 (Fig. 14c). It is useful for understanding the behaviors between the EM and INT to compare the NCEP observations with the EM, because the NCEP observations contain both SST-forced variability and internal variability.

Figure 14b compares the second PCs for the NCEP reanalysis and EM, and the Southern Oscillation Index (SOI). The EM-PC reproduces the NCEP observations reasonably, especially after 1976. The correlation between the EM and NCEP

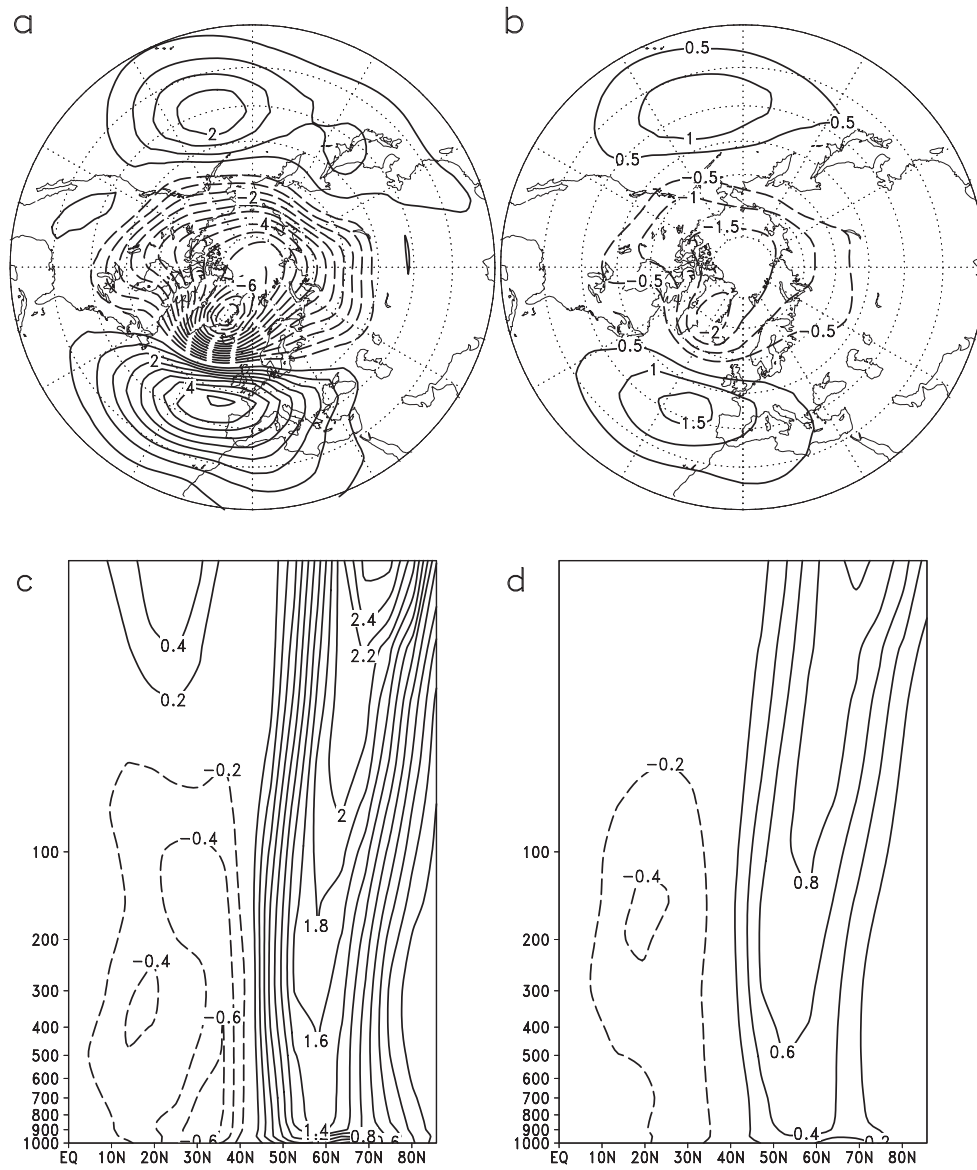


Fig. 13. EOF-1 of SLP anomalies (hPa) for DJF-mean based on (a) the data of all 20-member runs with the EM being subtracted each run (INT) and (b) EM (Same as in Fig. 6). Zonal-mean zonal wind (m s^{-1}) regressed on the SLP EOF-1 for (c) the INT and (d) EM. The contour interval is 0.5 hPa (a and b) and 0.2 m s^{-1} (c and d) with the zero contour omitted respectively.

PCs is seen both on interannual timescales and in the climate regime shift in the mid-1970s. Interestingly, the EM-PC is better correlated with the SOI (at 0.85) than with the NCEP-PC (at 0.21). For example, both the EM-PC and SOI take negative values in 1966 and 1969 while the NCEP-PC is positive. Likewise, the EM-PC and SOI are positive in 1974 and 1976 while the NCEP-PC is

weakly negative. This suggests that the observed PNA is excited by ENSO but contains internal variability as well, a result consistent with observational analysis (e.g., Zhang et al. 1996). The EM-PC correlates better with SOI than the NCEP-PC because it captures the ENSO-induced PNA-like wave train by averaging out chaotic variability.

Table 3. The maximum (minimum) in SLP EOF-1 (hPa) for EM and INT. Column 3 represents the ratio between the EM and total variance, with the bold type showing the above the 95% significance limit.

	EM	INT	variance ratio
Arctic	-2.38	-7.26	10.1
Atlantic	1.70	4.61	13.3
Pacific	1.49	2.37	32.1

5. Conclusions and discussion

We have conducted a 20-member ensemble simulation with an AGCM to study the patterns and

mechanisms for atmospheric variability in the winter Northern Hemisphere. The model reproduces the observed variance in SLP and upper tropospheric geopotential height in both spatial distribution and magnitude. We then divide the total variance into SST-induced component as represented by the EM and atmospheric internal variability as represented by intra-ensemble difference. The SST-forced component is potentially predictable to the extent that SST anomalies are predictable. The SST-forced variability is much greater over the North Pacific than the North Atlantic where internal variability dominates (with a small contribution from SST-induced variability in the subtropical

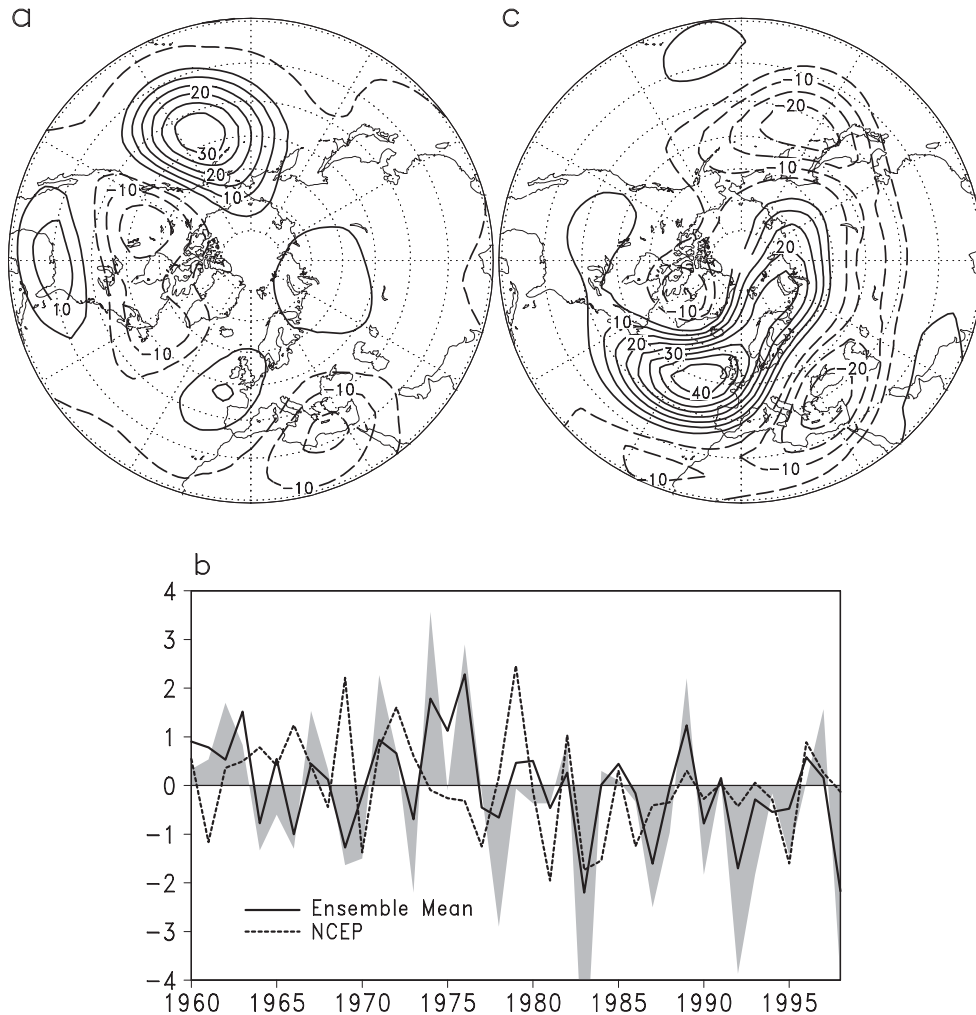


Fig. 14. DJF-mean 500 hPa geopotential height anomalies (m) regressed on the SLP EOF-2 for (a) EM and (c) INT. (b): The associated principal components for the NCEP reanalysis and EM, and the observed winter SOI (shading).

North Atlantic). Over the North Pacific, both SST-forced variability and internal variability contribute to the total variance.

AO-like patterns emerge as the leading EOF mode in both the EM and the entire time series of the 20 AGCM integrations with the EM being subtracted each run that is dominated by internal variability. The loading in the North Pacific is significantly greater (by one third) in the EM EOF than in the mode of the total (20×40 years) variability. Indeed, the correlation between the Pacific and Atlantic centers is larger in the EM than all but one member integration. This result suggests that while AO is an internal mode of the atmosphere, its response to global SST variability takes a different spatial pattern with enhanced coherence between North Pacific variability and Atlantic variability.

The winter EM-AO is forced by the North Pacific SST variability in autumn and winter, but the winter observed AO forces the North Pacific SST in winter and spring. Since there is a possibility that the North Pacific SST may force the AO, further study should be required for understanding the seasonal air-sea interaction in the North Pacific. In the North Atlantic, the winter AO is forced by the Barents-Kara sea-ice and Barents SST variability in autumn, in turn, forces the winter sea-ice cover in both the Labrador and Greenland Seas and weakens in the NAO sector. For this negative feedback, it is also suggested that the seasonal air-sea interaction plays an important role.

Observations capture only one realization of many possible climate variations, and include both internal variability and anomalies forced by slowly varying surface boundary conditions (e.g., Sugi et al. 1997). So far we have implicitly assumed that global SST variations are predictable. While tropical modes of SST variability such as ENSO are indeed predictable, much of SST anomalies in the extratropics is forced as a first-order Markov process by atmospheric internal variability. Thus the potential predictability discussed in this paper is almost certainly an overestimate (Barsugli and Battisti 1998; Bretherton and Battisti 2000). Conversely part of what we designated as internal variability may be predictable by exploiting the memory effects of soil moisture and snow cover over land. For example, Watanabe and Nitta (1998) and Gong et al. (2002) suggest that Siberian snow anomalies force AO-type variability in autumn and winter. While SST-forced variability in soil moisture and snow cover is captured in our ensemble

simulation, these land surface parameters are internal variables, not the prescribed variables. Further study would be required for understanding the responses of land and sea surface forcing on the decadal AO.

Acknowledgments

We thank M. Ikeda, T. Tokioka, M. Watanabe, and S. Minobe for helpful comments, and also two anonymous reviewers for providing useful comments. This work is supported by the JAMSTEC and NOAA CLIVAR Program. IPRC/SOEST publication #659/7856.

References

- Alexander, M. A., U. S. Bhatt, J. E. Walsh, M. S. Timlin, J. S. Miller, and J. D. Scott, 2004: The atmospheric response to realistic Arctic sea ice anomalies in an AGCM during winter. *J. Climate*, **17**, 890–905.
- Ambaum, M. H. P., B. J. Hoskins, and D. B. Stephenson, 2001: Arctic Oscillation or North Atlantic Oscillation. *J. Climate*, **14**, 3495–3507.
- Barsugli, J. J., and D. S. Battisti, 1998: The basic effects of atmosphere-ocean thermal coupling on midlatitude variability. *J. Atmos. Sci.*, **55**, 477–493.
- Bretherton, C. S., and D. S. Battisti, 2000: An interpretation of the results from atmospheric general circulation models forced by the time history of the observed sea surface temperature distribution. *Geophys. Res. Lett.*, **27**, 767–770.
- Cassou, C., and L. Terray, 2001: Oceanic forcing of the wintertime low-frequency atmospheric variability in the North Atlantic European sector: A study with the ARPEGE model. *J. Climate*, **14**, 4266–4291.
- Deser, C., 2000: On the Teleconnectivity of the “Arctic Oscillation”. *Geophys. Res. Lett.*, **27**, 779–782.
- Deser, C., J. E. Walsh, and M. S. Timlin, 2000: Arctic sea ice variability in the context of recent atmospheric circulation trends. *J. Climate*, **13**, 617–633.
- Feldstein, S. B., 2002: The recent trend and variance increase of the annular mode. *J. Climate*, **15**, 88–94.
- Gong, G., D. Entekhabi, and J. Cohen, 2002: A large-ensemble model study of the wintertime AO-NAO and the role of interannual snow perturbations. *J. Climate*, **15**, 3488–3499.
- Harzallah, A., and R. Sadourny, 1995: Internal versus SST-forced atmospheric variability as simulated by an atmospheric general circulation model. *J. Climate*, **8**, 474–495.
- Hoerling, M. P., J. W. Hurrell, and T. Xu, 2001: Tropical origins for recent North Atlantic climate change. *Science*, **292**, 90–92.

- Honda, M., and H. Nakamura, 2001: Interannual seesaw between the Aleutian and Icelandic lows. Part II: Its significance in the interannual variability over the wintertime Northern Hemisphere. *J. Climate*, **14**, 4512–4529.
- Honda, M., J. Inoue, and S. Yamane, 2009: Influence of low Arctic sea-ice minima on anomalously cold Eurasian winters. *Geophys. Res. Lett.*, **36**, L08707, doi:10.1029/2008GL037079.
- Hurrell, J. W., 1995: Decadal trends in the North Atlantic Oscillation: Regional temperatures and precipitation. *Science*, **269**, 676–679.
- Itoh, H., 2002: True versus apparent Arctic Oscillation. *Geophys. Res. Lett.*, **29**, 1268.
- Kalnay, E., M. Kanamitsu, and co authors, 1996: The NCEP/NCAR 40-year reanalysis project. *Bull. Amer. Meteor. Soc.*, **77**, 301–326.
- Kitoh, A., 1988: A numerical experiment on sea surface temperature anomalies and warm winter in Japan. *J. Meteor. Soc. Japan*, **66**, 515–533.
- Kushnir, Y., and I. M. Held, 1996: Equilibrium atmospheric response to North Atlantic SST anomalies. *J. Climate*, **9**, 1208–1220.
- Mehta, V. M., M. J. Suarez, J. V. Manganello, and T. L. Delworth, 2000: Oceanic influence on the North Atlantic Oscillation and associated Northern Hemisphere climate variations: 1959–1993. *Geophys. Res. Lett.*, **27**, 121–124.
- Numaguti, A., 1999: Origin and recycling processes of precipitating water over the Eurasian continent: Experiments using an atmospheric general circulation model. *J. Geophys. Res.*, **104**, 1957–1972.
- Numaguti, A., M. Takahashi, T. Nakajima, and A. Sumi, 1997: Description of CCSR/NIES atmospheric general circulation model. CGER Supercomputer Monograph Report. *Nat'l Inst. for Environ. Studies, Tsukuba*, **3**, 1–48.
- Okumura, Y., and S.-P. Xie, 2003: Atmospheric response to tropical Atlantic SST anomalies: Role of planetary boundary layer adjustment. *Proc. 12th Conf. on the interaction of the Sea and Atmos.*, P2.1, Amer. Meteor. Soc., Boston, 1–7.
- Okumura, Y., S.-P. Xie, A. Numaguti, and Y. Tanimoto, 2001: Tropical Atlantic air-sea interaction and its influence on the NAO. *Geophys. Res. Lett.*, **28**, 1507–1510.
- Palmer, T. N., and Z. Sun, 1985: A modelling and observational study of the relationship between sea surface temperature in the northwest Atlantic and the atmospheric general circulation. *Quart. J. Roy. Meteor. Soc.*, **111**, 947–975.
- Peng, S., W. A. Robinson, and M. P. Hoerling, 1997: The modeled atmospheric response to midlatitude SST anomalies and its dependence on background circulation states. *J. Climate*, **10**, 971–987.
- Quadrelli, R., and J. M. Wallace, 2002: Dependence of the structure of the Northern Hemisphere annular mode on the polarity of ENSO. *Geophys. Res. Lett.*, **29**, 2132, doi:10.1029/2002GL015807.
- Rayner, N. A., E. B. Horton, D. E. Parker, C. K. Folland, and R. B. Hackett, 1996: *Version 2.2 of the global sea-ice and sea surface temperature data set*.
- Rodwell, M. J., D. P. Rowell, and C. K. Folland, 1999: Oceanic forcing of the wintertime North Atlantic Oscillation and European climate. *Nature*, **398**, 320–323.
- Rowell, D. P., 1998: Assessing potential seasonal predictability with an ensemble of multidecadal GCM simulations. *J. Climate*, **11**, 109–120.
- Rowell, D. P., C. K. Folland, K. Maskell, and M. N. Ward, 1995: Variability of summer rainfall over tropical north Africa (1906–92): Observations and modelling. *Quart. J. Roy. Meteor. Soc.*, **121**, 669–704.
- Schneider, N., and A. J. Miller, 2001: Predicting western North Pacific Ocean climate. *J. Climate*, **14**, 3997–4002.
- Schneider, E. K., L. Bengtsson, and Z. Z. Hu, 2003: Forcing of Northern Hemisphere climate trends. *J. Atmos. Sci.*, **60**, 1504–1521.
- Sugi, M., R. Kawamura, and N. Sato, 1997: A study of SST-forced variability and potential predictability of seasonal mean fields using the JMA global model. *J. Meteor. Soc. Japan*, **75**, 717–736.
- Thompson, D. W. J., and J. M. Wallace, 1998: The Arctic Oscillation signature in the wintertime geopotential height and temperature fields. *Geophys. Res. Lett.*, **25**, 1297–2000.
- Thompson, D. W. J., and J. M. Wallace, 2000: Annular modes in the extratropical circulation. Part I: Month-to-month variability. *J. Climate*, **13**, 1000–1016.
- Wallace, J. M., and D. S. Gutzler, 1981: Teleconnections in the geopotential height field during the Northern Hemisphere winter. *Mon. Wea. Rev.*, **109**, 784–812.
- Watanabe, M., and T. Nitta, 1998: Relative impacts of snow and sea surface temperature anomalies on an extreme phase in the Winter atmospheric circulation. *J. Climate*, **11**, 2837–2857.
- Xie, S. P., H. Noguchi, and S. Matsumura, 1999: A hemispheric-scale quasi-decadal oscillation and its signature in Northern Japan. *J. Meteor. Soc. Japan*, **77**, 573–582.
- Xie, S. P., T. Kunitani, A. Kubokawa, M. Nonaka, and S. Hosoda, 2000: Interdecadal thermocline variability in the North Pacific for 1958–1997: A GCM simulation. *J. Phys. Oceanogr.*, **30**, 2798–2813.
- Yamamoto, K., Y. Tachibana, M. Honda, and J. Ukita,

- 2006: Intra-seasonal relationship between the Northern Hemisphere sea ice variability and the North Atlantic Oscillation. *Geophys. Res. Lett.*, **33**, L14711, doi:10.1029/2006GL026286.
- Yamazaki, K., and Y. Shinya, 1999: Analysis of the Arctic Oscillation simulated by AGCM. *J. Meteor. Soc. Japan*, **77**, 1287–1298.
- Zhang, Y., J. M. Wallace, and N. Iwasaka, 1996: Is climate variability over the North Pacific a linear response to ENSO? *J. Climate*, **9**, 1468–1478.